2025 SCEC Project Report

Detailed V_P and V_S Model, and Seismicity Catalog of the Mina Deflection Region of the Central Walker Lane from a Rapid Nodal Deployment

SCEC Award No. **25192**

PI: Patricia Persaud, University of Arizona

Graduate Student:
Joses Omojola, University of Arizona

Proposal Categories:
Individual Research Project

Disciplinary Group:
Seismology, Plate Boundary System, Community Earth Models

SCEC Science Milestones:
A1-3, A2-3, A3-2, D1-1

ABSTRACT

The 2020 Mw 6.5 Monte Cristo Range earthquake occurred in the California-Nevada border region. The earthquake occurred on a previously unmapped fault, in the Central Walker Lane. The Walker Lane and Eastern California Shear Zone can be considered a natural laboratory outside the most populated regions of California for SCEC to consider issues of seismicity and fault mechanics (e.g., Wesnousky, 2024). The USGS rapidly deployed 60 three-component nodal seismic instruments to monitor the aftershock sequence and data were recorded for one month. Using EQTransformer for automatic event detection and phase picking, we have produced a high-resolution catalog of the aftershocks. Detections occurring on at least 10 stations were classified as events. Our preliminary results show that over 19,400 events occurred in the 1-month period. Compared to the Ruhl et al. catalog of 16,714 events from eight stations that recorded for 3.5 months, our initial catalog contains 16% more events with increased ray path density across the aftershock area. In this study, we refine our preliminary work to produce a high-fidelity earthquake catalog, and large-scale and high-resolution 3D P-wave and S-wave travel-time tomographic models from the phase picks (Figure 1). The large-scale and high-resolution tomographic models are genetically related. As such they are a critical step toward muti-scale models for the Central Walker Lane. We also carry out gravity modeling informed by our tomographic model to determine density and sediment thicknesses. The velocity, sediment thickness and density models in the CA-NV border region are available for inclusion in statewide Earth models.

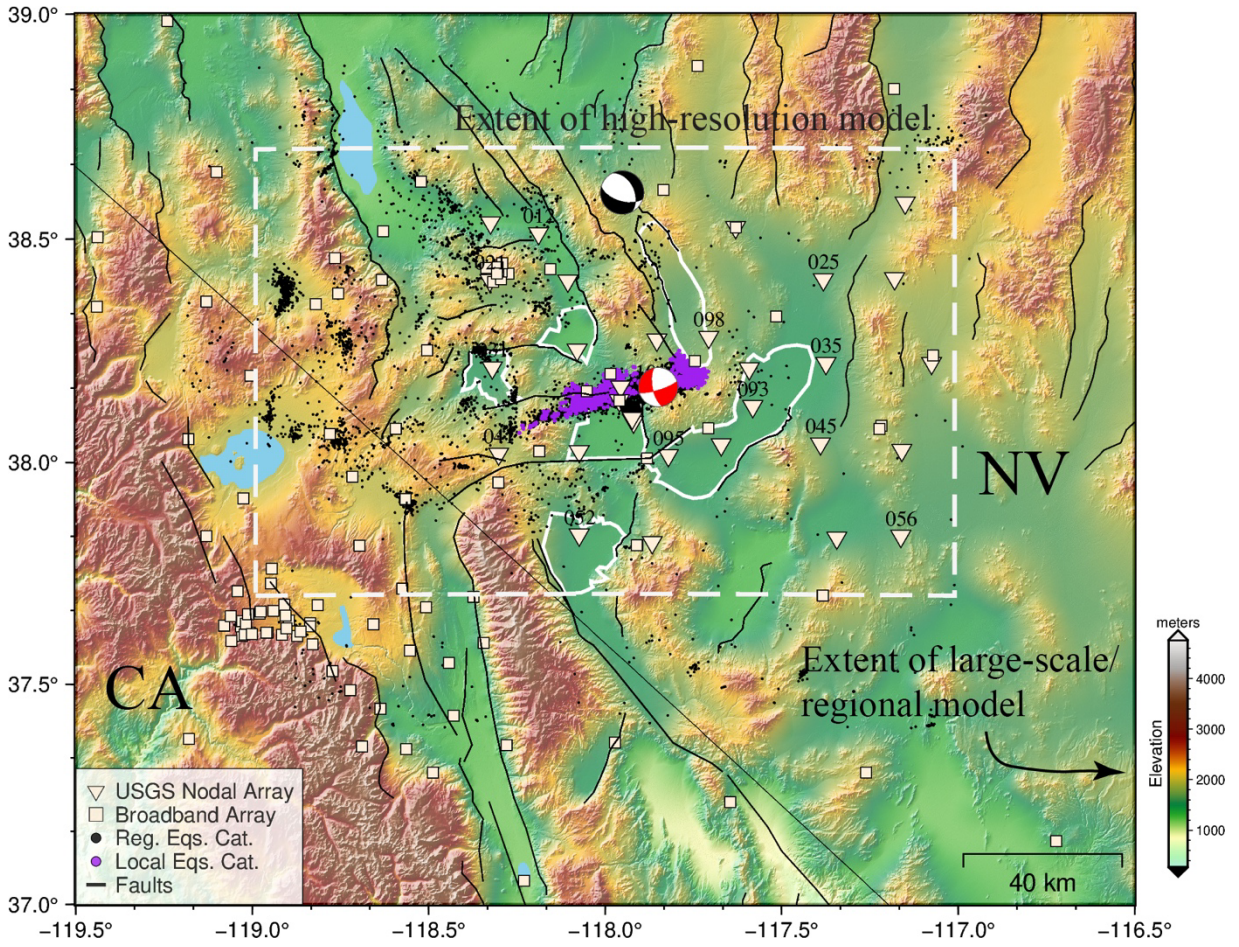

Figure 1. *Seismic stations and events (earthquakes and mine blasts) used in our multi-scale travel time 3D velocity models. The full map extent is equivalent to the large-scale model which is also shown in Figure 2 and the high-resolution model extent is shown with the white dashed rectangle. Earthquakes above magnitude 3 from 2010-2022 are shown as black dots USGS (2025) and relocated earthquakes from our deep-learning earthquake catalog are shown as purple dots. The black focal mechanism is for the 1932 Cedar Mountain M7.2 earthquake. The red focal mechanism is for the 2020 M_w 6.5 Monte Cristo Range earthquake. Black lines are surface traces of mapped faults from Oldow, (1992) and Wesnousky, (2005). Sedimentary basins are outlined in white.*

METHODOLOGY

We developed integrated 3D seismic velocity (V_P, V_S, and V_P/V_S) and density models of the Central Walker Lane using local earthquake tomography applied to aftershocks from the 2020 M_w 6.5 Monte Cristo Range earthquake and gravity inversion. Our seismic dataset consists of continuous waveforms from 60 nodal stations deployed by the USGS following the mainshock (Goldman et al., 2023). We employed the deep-learning-based EQTransformer model to detect phase arrivals (Mousavi et al., 2020). We located events using HYPOINVERSE with a minimum of 4 stations per event and relocated them using HypoDD with double-difference constraints for event pairs separated by less than 3 km (Klein, 2002; Waldhauser, 2001). To address challenges in using automated phase picks for tomography, we implemented an iterative quality control approach that filters uncorrelated phase picks using a 3D eikonal ray tracer. Our filtering process was repeated until event locations stabilized and no additional picks were rejected, yielding a high-quality catalog of over 9,600 aftershocks. To expand ray path coverage around our study area and at depth, we also included phase picks at available broadband stations shown in Figure 1.

We inverted travel times for our body-wave arrivals using the finite-difference travel-time tomography method of Hole (1992) and Hole & Zelt (1995). Because no community velocity model has been previously developed for the Central Walker Lane, we adopted a multi-resolution inversion strategy. This approach allows our high-resolution model covering the aftershock region to be readily merged with our large-scale or regional model since they are both derived from similar datasets using a common method. First, using a smoothed 1D model of Ruhl et al. (2021) as the starting model, we inverted a declustered subset of events on a coarse grid (5 km grid cells) to recover a minimum-structure velocity model referred to as our large-scale model. The large-scale model covers a 330 km x 220 km region overlapping the California-Nevada border (Figures 1 and 2). This coarse parameterization ensures individual cells are well-constrained by multiple ray paths. In the second stage, we used the large-scale P- and S-wave models as starting models for high-resolution inversions (1 km grid cells), incorporating our full high-quality phase pick dataset. The high-resolution model covers an ~220 km x 110 km region in the Central Walker Lane (white dashed rectangle in Figure 1). To quantify model non-uniqueness, we systematically varied smoothing parameters, regridding schemes, earthquake ordering, number of inversion cycles, and starting models, generating an ensemble of 120 equally probable solutions from 21,870 possible parameter combinations. Further, to improve constraints on shallow crustal structure where ray path coverage from local earthquake tomography is limited, we inverted Bouguer gravity anomalies using the SimPEG library (Cockett et al., 2015). We generated a reference density model by converting our final P-wave velocity model to density using the empirical relationship

of Brocher (2005). Finally, we employed L2-norm regularization and used Gauss-Newton optimization until convergence.

RESULTS

Our relocated earthquake catalog reveals tightly clustered seismicity aligned with the eastward extension of the Candelaria Hills fault, extending over 25 km east until intersecting the Petrified Springs fault. The faulted area can be differentiated into two distinct zones: an ENE-trending main zone (left-lateral) and a NW-SE-trending minor zone (right-lateral), consistent with focal mechanisms from previous studies (Ruhl et al., 2021).

The large-scale P-wave velocity model reveals a heterogeneous upper crust with velocities ranging from 3-4.5 km/s in sedimentary basins to 5-6.5 km/s in mountain ranges (Figure 2). Ray coverage extends from the surface to 20 km depth. Comparison with the CANVAS adjoint waveform tomography model (Doody et al., 2023) showed our model captures substantially more structural detail despite the similar grid spacing. The CANVAS model shows minimum velocities of 5.5 km/s and fails to image sedimentary basins or velocity contrasts across mapped fault blocks. Our S-wave model differentiates basins ($V_S < 2.5$ km/s) from ranges ($V_S > 3.8$ km/s) more clearly than V_P. Computed V_P/V_S ratios range from 1.4 to 1.8, with elevated ratios (>1.734) beneath the Long Valley Caldera and Mono craters. Below 12 km depth, decreased seismicity coincides with the 1.69 V_P/V_S contour, consistent with the brittle-ductile transition mapped by previous studies.

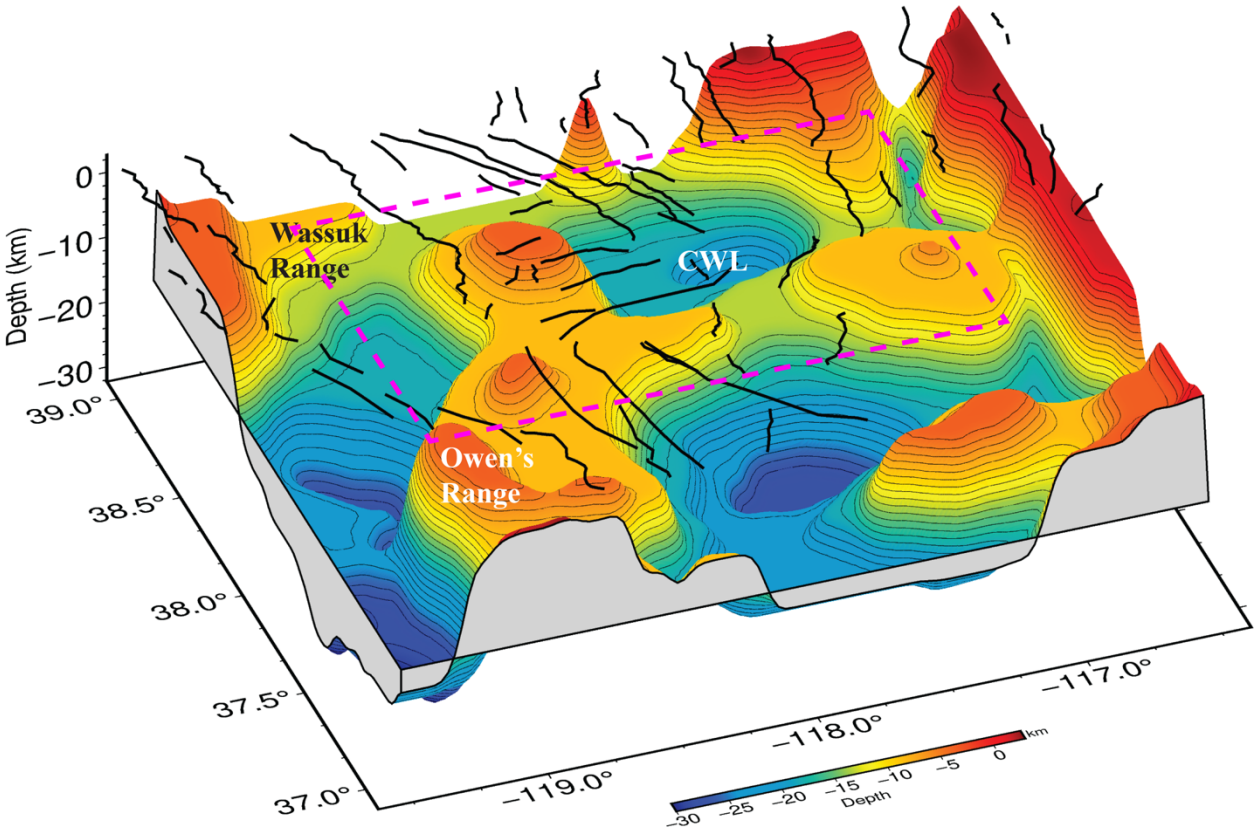

Figure 2. *3D perspective view from the southeast of the V_P = 6.4 km/s iso-velocity surface obtained from our large-scale V_P model in the CA-NV border region. The iso-velocity surface highlights major mountain ranges across the study area. The pink dashed rectangle marks the location of our high-resolution model covering the Central Walker Lane (CWL) region including the aftershock region of the 2020 M_w 6.5 Monte Cristo Range earthquake.*

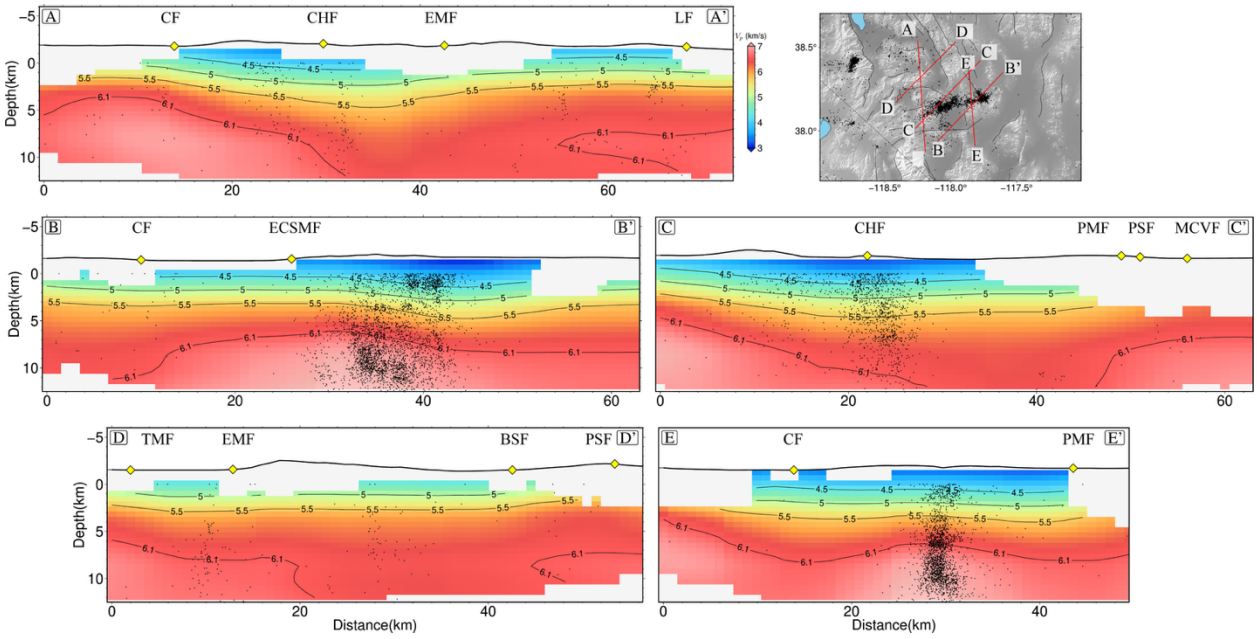

Figure 3. *Vertical profiles from our final high-resolution V_P model showing velocity contrasts across fault blocks of the Central Walker Lane. Profile locations are shown in the inset map. Areas with no ray coverage are masked out. Fault intersections along the vertical profiles are shown with yellow diamonds. BSF – Benton Springs Fault; CF - Coaldale Fault; CHF - Candeleria Hills Fault; ECSMF – East Candeleria Salt Marsh Fault; EMF – Excelsior Mountain fault; MCVF – Monte Cristo Valley Fault; PSF - Petrified Springs Fault; PMF - Pilot Mountain Fault; TMF – Teels Marsh Fault; WRF - Wassuk Range Fault.*

Our high-resolution P-wave velocity model highlights prominent lateral heterogeneities and fills imaging gaps within the Central Walker Lane (Figure 3). The smaller grid size successfully resolves narrow mountain ranges like the Wassuk Range (V_P > 6.4 km/s) that were unresolved in the coarser model. Good ray coverage extends from 3 to 12 km depth, with seismic velocities in the sedimentary basin ranging from 3.5 to 4.5 km/s in regions of high station and event density. The high-resolution V_P/V_S model reveals distinct fault-bounded anomalies between 3 and 5 km depth. Integration of velocity and density models shows distinct subsurface features that were not apparent from either dataset independently. The 3D density contrast model from our gravity inversion successfully delineates sedimentary basins with low density contrast values (< -0.3 g/cm^3) aligned with mapped basin extents. This provides crucial constraints at shallow depths (<5 km) where ray path coverage is limited, particularly east of longitude -117.5° where station density

is sparse. Finally, our ensemble approach quantifies velocity uncertainties across the model domain. Standard deviations ranged from <0.05 km/s in well-sampled regions to >0.15 km/s in areas with sparse ray coverage, providing confidence bounds for interpretations and engineering applications.

INTELLECTUAL MERIT

Our study contributes to the SCEC mission of analyzing data from field observations and developing subsurface multi-scale models for improving understanding of seismic hazards. We've developed the first multi-scale 3D models with quantified uncertainties, that image the geometry and depth of six sedimentary basins in the Central Walker Lane. Our models resolve rheological transitions within the crust that directly impact earthquake nucleation. They provide insights into deformation along recent transtensional fault zones thereby contributing to our understanding of immature fault systems. Our multi-scale velocity models, density model and earthquake catalog will accompany the peer review publication.

BROADER IMPACTS

This project involved a PhD student and a postdoctoral researcher. A new method was developed in this study that produces a full suite of multiscale Earth models (V_P, V_S, V_P/V_S, density) with uncertainties for the Central Walker Lane. The models draw on diverse datasets (seismic and gravity) and a newly created deep-learning earthquake catalog produced from nodal array recordings. This approach can be readily applied to other SCEC focus areas to help improve ground motion predictions. The results from this research have been used in presentations and lectures given by the PI and other project participants.

PEER-REVIEWED PUBLICATIONS RESULTING FROM THIS AWARD

Omojola, J., & Persaud, P. (2025). Multiscale Seismic Tomography and Gravity Modeling of the Central Walker Lane, Nevada from a Deep-Learning Earthquake Catalog. In preparation for submission to Journal of Geophysical Research: Solid Earth, May 2025.

PRESENTATIONS RELATED TO THIS PROJECT

Persaud, P., Omojola J., Catchings R., & Goldman M., (2025). Exploring the Cross-Fault Rupture Zone of the 2020 Mw 6.5 Monte Cristo Range Earthquake of the Central Walker Lane. Poster Presentation at 2025 SCEC Annual Meeting. SCEC Contribution 14690.

Omojola J., Persaud, P., Nardoni C. & Catchings R., (2022). Utilizing Automated Picks from the 2020 Mw 6.5 Monte Cristo Range Earthquake Sequence to Image the Aftershock Region. Poster Presentation at 2022 SCEC Annual Meeting. SCEC Contribution 12075.

REFERENCES

Brocher, T. M. (2005, 12). Empirical relations between elastic wavespeeds and density in the Earth's crust. Bulletin of the Seismological Society of America, 95 (6), 2081-2092.

Cockett, R., Kang, S., Heagy, L. J., Pidlisecky, A., & Oldenburg, D. W. (2015). Simpeg: An open source framework for simulation and gradient based parameter estimation in geophysical applications. Computers Geosciences, 85 , 142-154.

Doody, C., Rodgers, A., Afanasiev, M., Boehm, C., Krischer, L., Chiang, A., & Simmons, N. (2023). Canvas: An adjoint waveform tomography model of california and nevada. Journal of Geophysical Research: Solid Earth, 128 (12), e2023JB027583.

Goldman, M. R., Catchings, R. D., Chan, J. H., & Criley, C. J. (2023). Three component nodal recordings of aftershocks from the 15 may 2020 Mw 6.5 Monte Cristo, Nevada earthquake [Dataset]. US Geological Survey (USGS) Data Release. doi.10.5066/P9Z3UE7I

Hole, J. A. (1992). Nonlinear high-resolution three-dimensional seismic travel time tomography, Journal of Geophysical Research: Solid Earth, 97 (B5), 6553-6562.

Hole, J. A., Brocher, T. M., Klemperer, S. L., Parsons, T., Benz, H. M., & Furlong, K. P. (2000). Three-dimensional seismic velocity structure of the San Francisco bay area. Journal of Geophysical Research: Solid Earth, 105 (B6), 13859-13874.

Hole, J. A., & Zelt, B. C. (1995, 05). 3-D Finite-difference reflection travel-times. Geophysical Journal International , 121 (2), 427-434.

Klein, F. W. (2002). User's guide to hypoinverse-2000, a fortran program to solve for earthquake locations and magnitudes (Software No. 2331-1258). US Geological Survey.

Mousavi, S. M., Ellsworth, W. L., Zhu, W., Chuang, L. Y., & Beroza, G. C. (2020). Earthquake transformer—an attentive deep-learning model for simultaneous earthquake detection and phase picking. Nature communications, 11 (1), 1–12. doi: 10.1038/s41467-020-17591-w

Oldow, J. S., & Craig, S. (1992). Late cenozoic displacement partitioning in the northwestern great basin. In Geological Society of Nevada Walker Lane Symposium: Structure, tectonics and mineralization of the walker lane: Reno, Geological Society of Nevada (p. 17–52).

Ruhl, C. J., Morton, E. A., Bormann, J. M., Hatch-Ibarra, R., Ichinose, G., & Smith, K. D. (2021). Complex fault geometry of the 2020 M_{ww} 6.5 Monte Cristo Range, Nevada, earthquake sequence. Seismological Research Letters, 92 (3), 1876–1890.

USGS. (2025). USGS earthquakes catalog Retrieved 2026-03-02, from https://earthquake.usgs.gov/earthquakes/search

Waldhauser, F. (2001). Hypodd - A program to compute double-difference hypocenter locations (Software No. 2331-1258). Retrieved from https://doi.org/10.3133/ofr011131015

Wesnousky, S. G. (2005), Active faulting in the Walker Lane, Tectonics, 24, TC3009, doi:10.1029/2004TC001645.

Wesnousky, S. G. (2024). The Walker Lane and Eastern California Shear Zones. Oral Presentation at 2024 SCEC Annual Meeting.